Supplementary Information

Lateral heterojunctions within ultrathin FeS-FeSe$_2$ nanosheet semiconductors for photocatalytic hydrogen evolution reaction

Jia Jia[a], Qiqi Zhang[a], Zong Li[a], Xiaoyun Hu[b], Enzhou Liu[a,*], and Jun Fan[a,*]

[a]School of Chemical Engineering, Northwest University, Xi'an 710069, P. R. China.

[b]School of Physics, Northwest University, Xi'an 710069, P. R. China.

*Corresponding author. Tel.: +86 29 88303679; fax: +86 29 88302223.

E-mail address: fanjun@nwu.edu.cn; liuenzhou@nwu.edu.cn

As shown in Fig. S1a, the characteristic peaks at 29.26°, 31.16°, 34.86°, 36.28°, 44.58°, 48.31°, 53.94°, 57.58° and 64.14° are preciously attributed to (011), (101), (111), (120), (121), (211), (031), (131) and (122) crystal planes of orthorhombic $FeSe_2$ (JCPDS 21-0432). There are no other XRD diffraction patterns from pyrrhotite FeS sample (JCPDS: 37-0477). Meanwhile, it can be seen from Fig. S1b that the $FeS_{2-x}Se_2$ composite shows a thicker and larger nanosheet morphology, which is different from pure $FeSe_2$, FeS and $FeS-FeSe_2$ heterostructures.
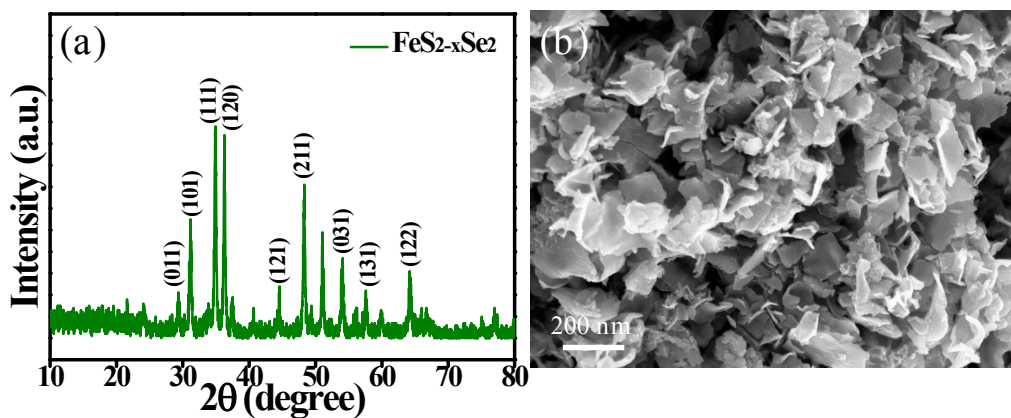

Fig. S1 (a) XRD pattern and (b) SEM image of the $FeS_{2-x}Se_2$ sample.
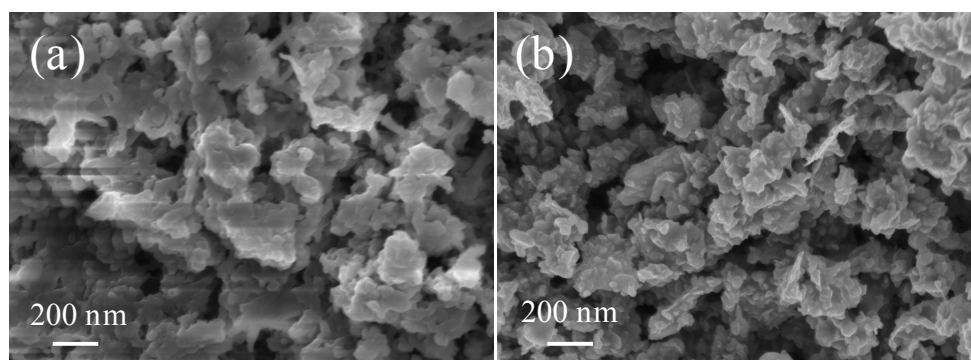

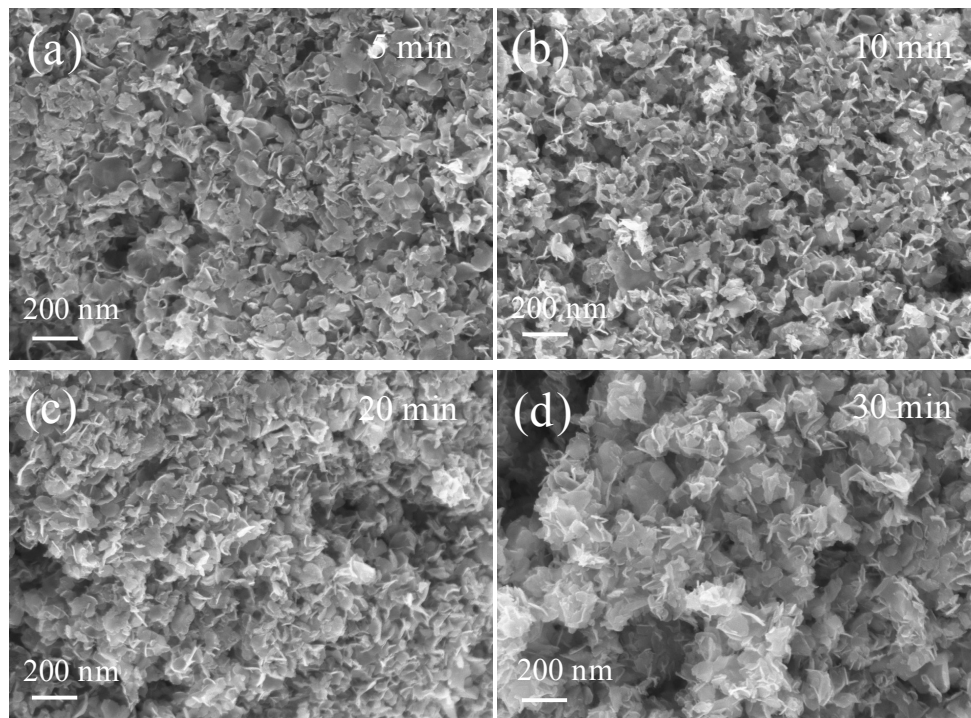**Fig. S2** The SEM picture of FeS at different temperature: (a) 200 °C and (b) 225 °C.

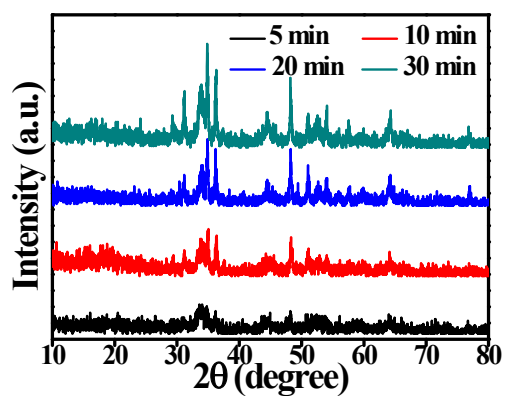**Fig. S3** The SEM picture of FeS-FeSe$_2$ heterostructure at different reaction time.

Fig. S4 The XRD pattern of FeS-FeSe$_2$ heterostructure at different reaction time.

Table S1. The BET specific surface areas of different samples.

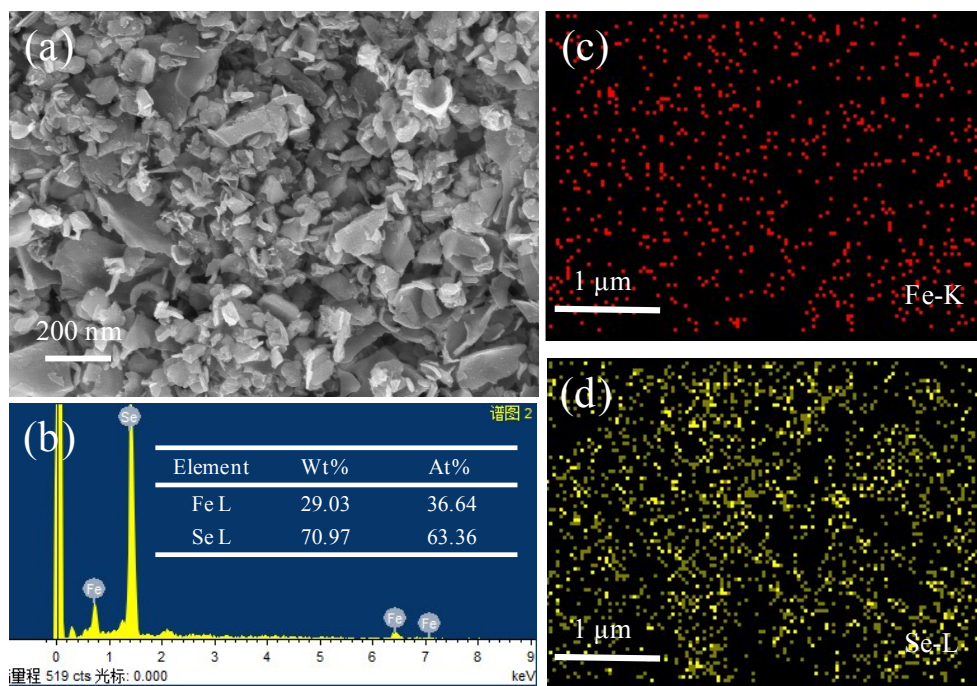| Samples	S_{BET} (m^2/g)	Average pore size (nm)	Pore volume (cm^3/g)
FeSe$_2$	17.77	3.708	0.098
FeS-FeSe$_2$	52.99	3.372	0.229
FeS	41.07	3.760	0.244

Fig. S5 The SEM (a), EDS (b), and EDS Mapping (c) picture for as-prepared $FeSe_2$ samples.
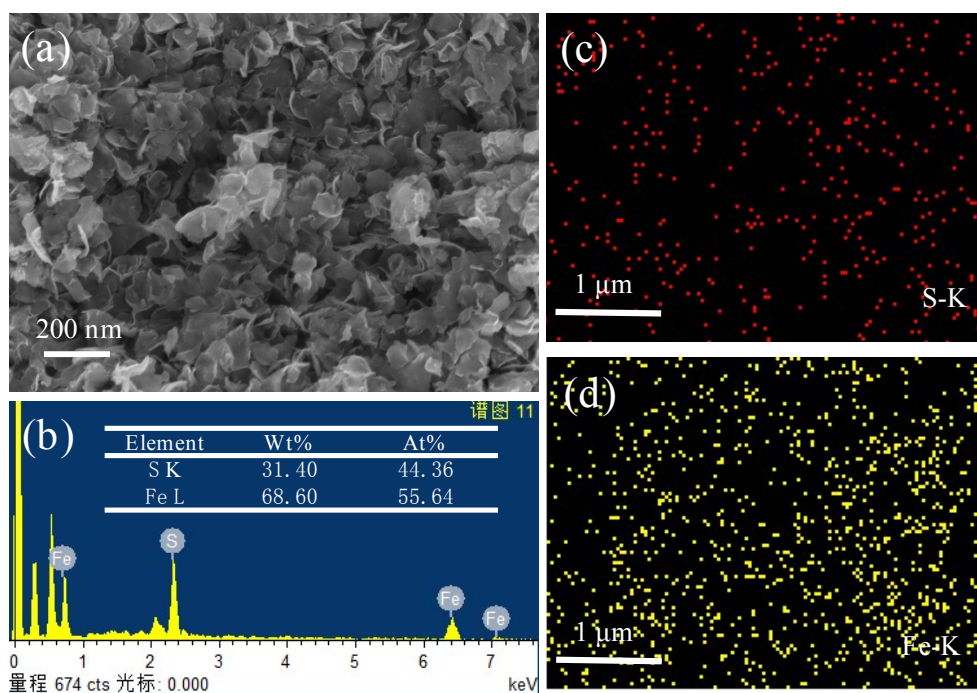

Fig. S6 The SEM (a), EDS (b), and EDS Mapping (c) picture for as-prepared FeS samples.

The TEM, HRTEM image and corresponding SAED pattern of pure FeS and $FeSe_2$ are shown in Fig. S7. The pure FeS and $FeSe_2$ shows a well-defined 2D sheet-like structure, while FeS nanosheet is obviously thinner than that of $FeSe_2$ (Fig. S7a and b). The HRTEM (Fig. S7c and d) images exhibit that the d-space distance of 0.265 nm can be assigned to the (112) plane of pyrrhotite FeS, and those of 0.256 nm can be attributed to the (111) plane of orthorhombic $FeSe_2$. The corresponding SAED patterns of FeS and FeSe2 demonstrate they have well-crystallized single crystal (the inset of Fig. S7c and d), which are in accordance with the XRD analysis.
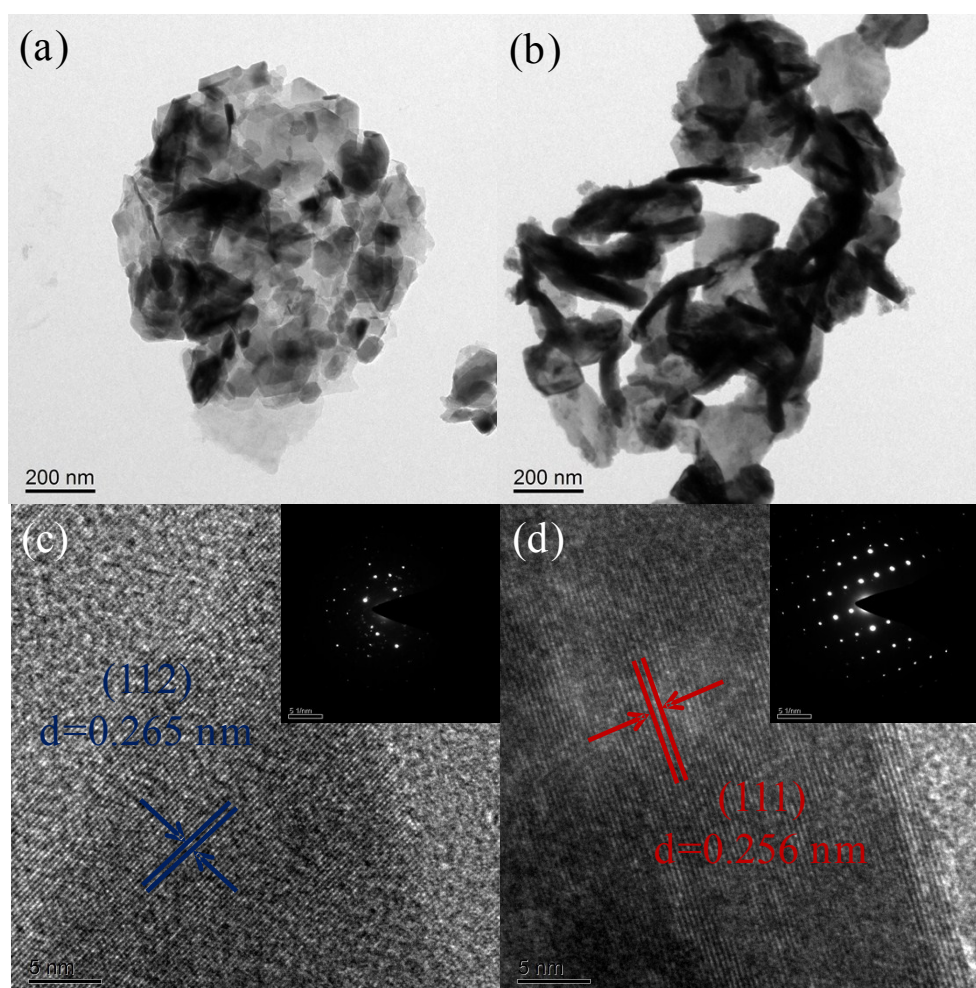

Fig. S7 The TEM and HRTEM (the inset of SAED pattern) images of pure (a, c) FeS and (b, d) $FeSe_2$.
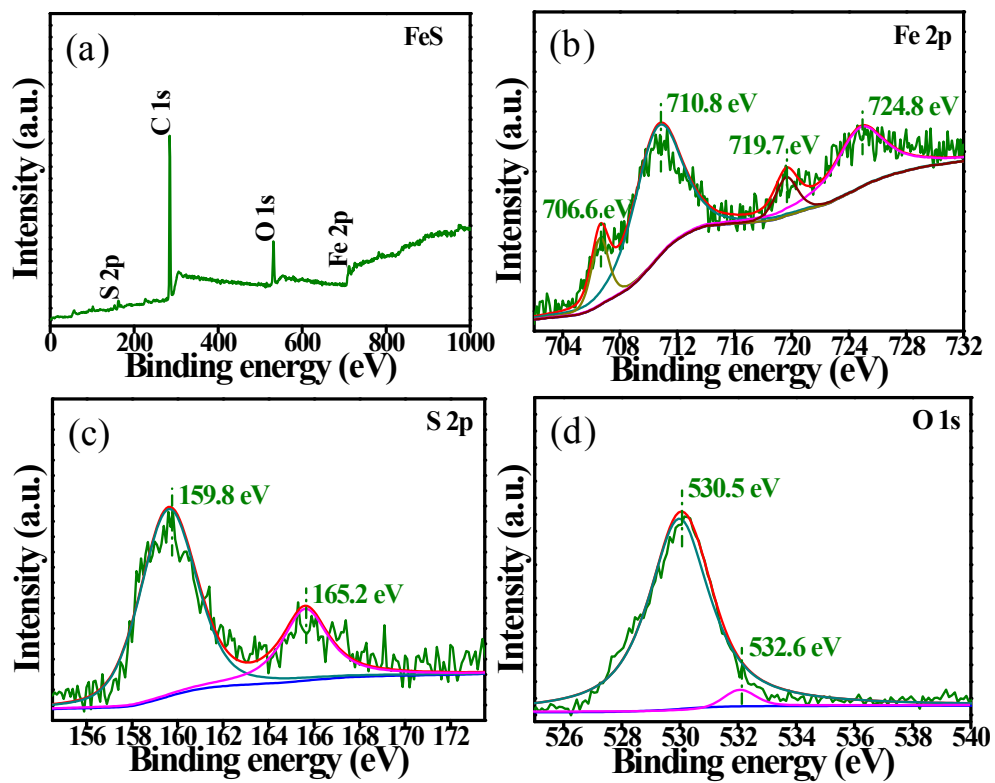
Fig. S8 (a) XPS survey spectra and the corresponding high-resolution XPS spectra of (b) Fe 2p, (c) S 2p and (d) O 1s for the FeS sample.
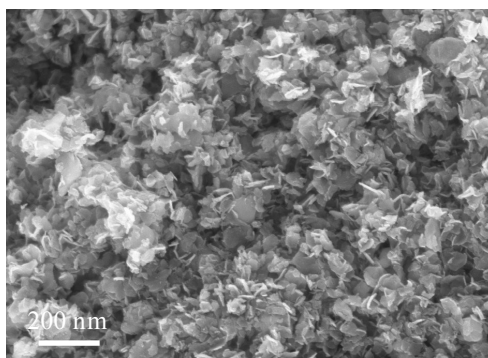

Fig. S9 The SEM for FeS-FeSe$_2$ samples after cycling H$_2$ evolution.
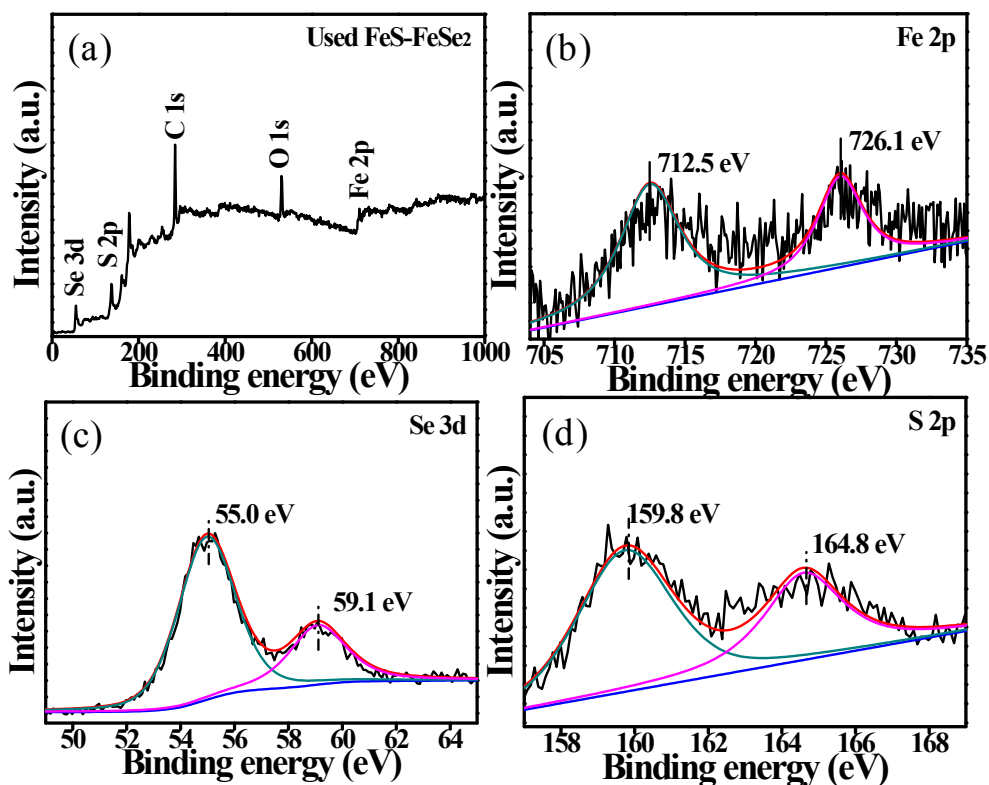
Fig. S10 (a) XPS survey spectra and the corresponding high-resolution XPS spectra of (b) Fe 2p, (c) Se 3d and (d) S 2p for FeS-FeSe$_2$ samples after cycling H$_2$ evolution.

Compared with FeSe$_2$, the FeS-FeSe$_2$ shows stronger adsorption ability, the relative concentration of MB and Cr(VI) molecules can remain 89.5% and the 82.6% after stirring in the dark for 180 min, respectively. The corresponding rate constant of k are calculated as 5.48×10^{-4} and 1.05×10^{-3} min^{-1} for the FeS-FeSe$_2$, which are higher than that of FeSe$_2$ (Fig. S11a and Fig. S12). The absorption ability of the catalysts for RhB and Cr(VI) are similar to the above results. The 88.9% of RhB and 87.8% of Cr(VI) remain in the solution with the addition of the FeS-FeSe$_2$ composite. The adsorption rate constant are determined to 6.85×10^{-4} and 8.5×10^{-4} min^{-1} for FeS-FeSe$_2$, respectively (Fig. S11b and Fig. 13). The strong absorption ability of the FeS-FeSe$_2$ composites will play an important role in the photocatalytic redox reaction process. The key adsorption data are shown in Table S2.

Table S2. The key adsorption data of the FeSe$_2$ and FeS-FeSe$_2$ samples.

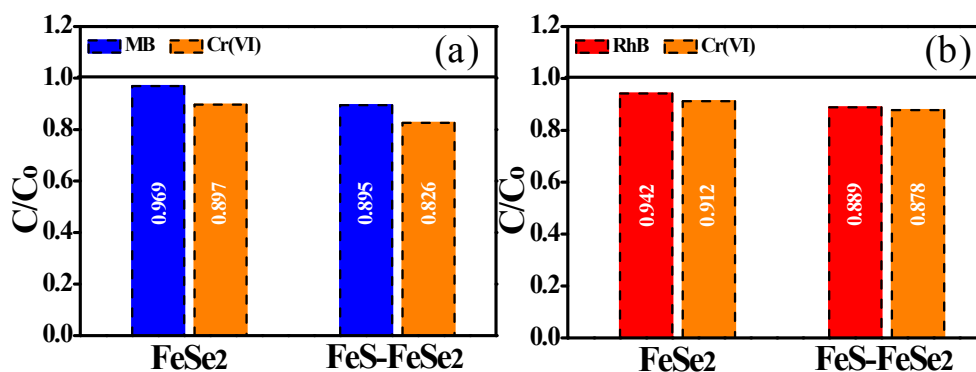| Sample	Relative Remaining Concentration (C/C$_o$)		Rate Constant (×10^{-4} min^{-1})	
	MB/Cr(VI)	RhB/Cr(VI)	MB/Cr(VI)	RhB/Cr(VI)
FeSe$_2$	96.9%/89.7%	94.2%/91.2%	1.28/6.55	3.16/5.42
FeS-FeSe$_2$	89.5%/82.6%	88.9%/87.8%	5.48/10.5	6.85/8.5

Fig. S11 The relative remaining concentration (C/C_o) of the dye and Cr(VI) for pure FeSe$_2$ and FeS-FeSe$_2$ materials after stirring in the dark for 180 min.
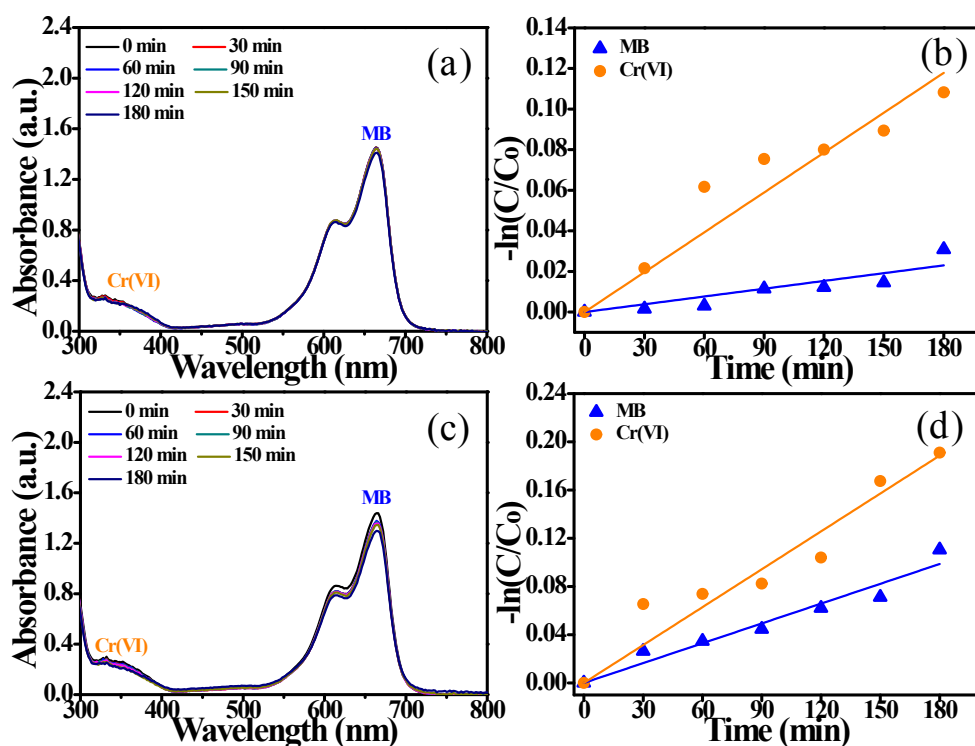

Fig. S12 The adsorption ability at different times and corresponding rate constant of pure FeSe$_2$ (a, b) and FeS-FeSe$_2$ (c, d) materials for methylene blue (MB, adsorption peak at 654 nm) and Cr(VI) (adsorption peak at 354 nm).
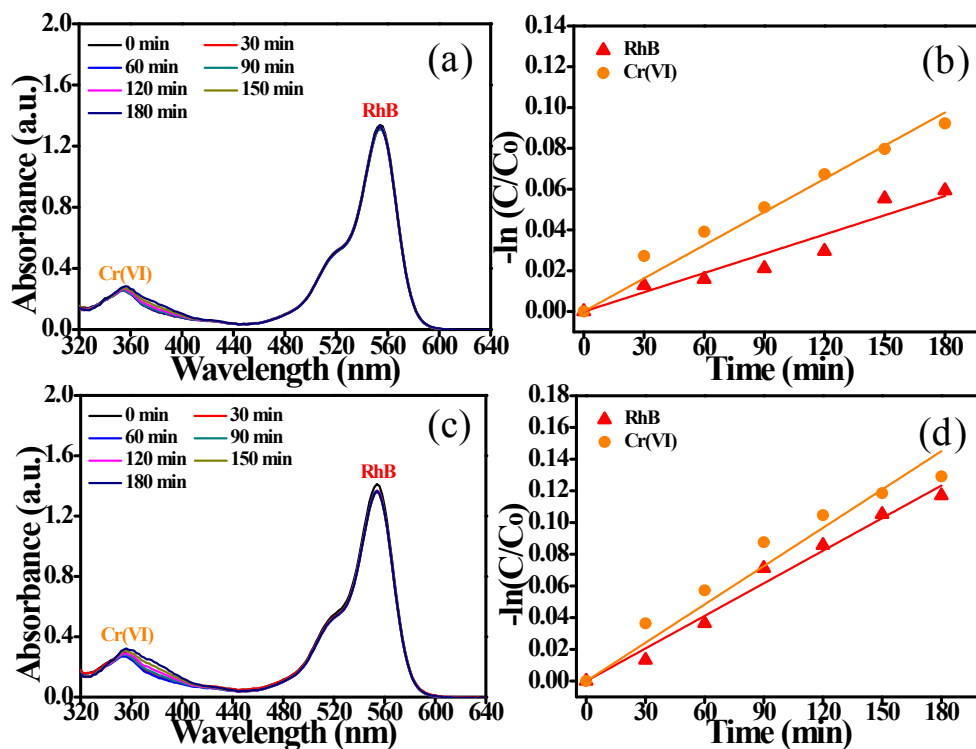
Fig. S13 The adsorption ability at different times and corresponding rate constant of pure FeSe$_2$ (a, b) and FeS-FeSe$_2$ (c, d) materials for rhodamine B (RhB, adsorption peak at 554 nm) and Cr(VI) (adsorption peak at 354 nm).
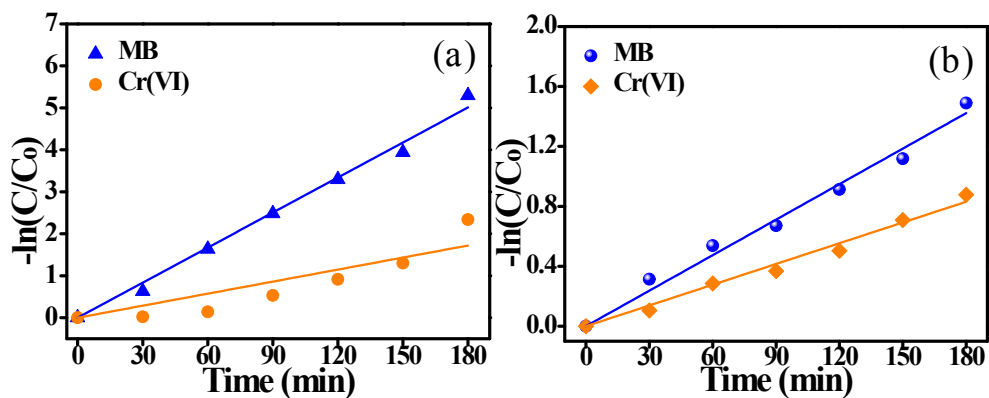

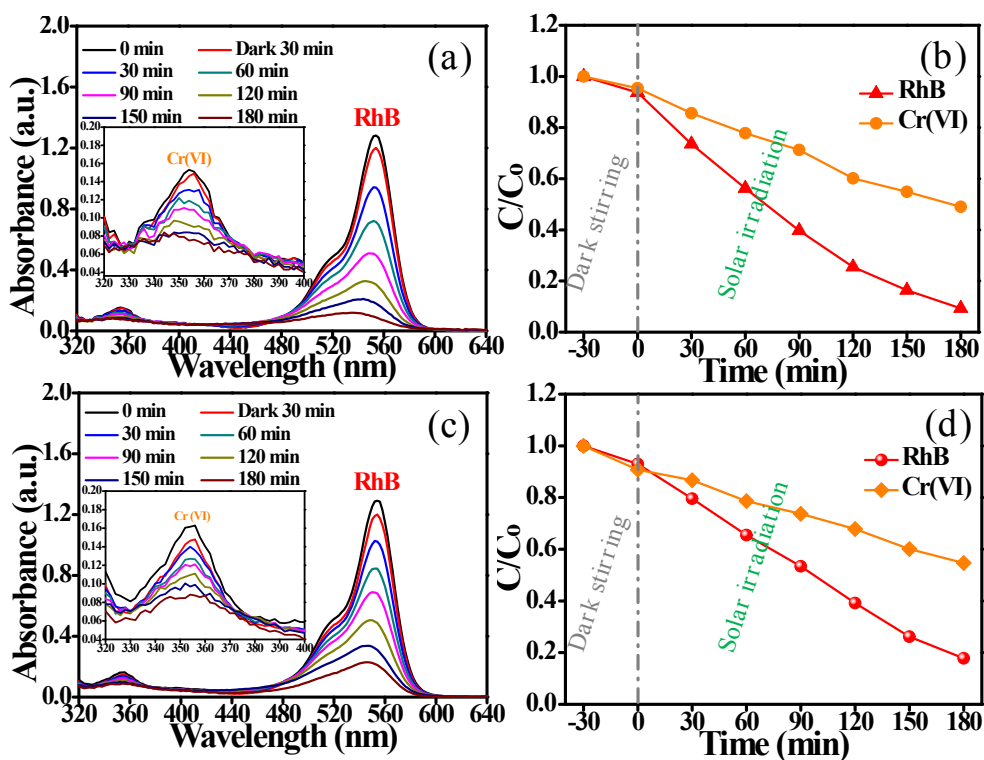**Fig. S14** The MB and Cr(VI) removal rate constant for the (a) FeS-FeSe$_2$ and (b) FeSe$_2$.

Fig. S15 Photocatalytic activity of FeS-FeSe$_2$ (a, b) and FeSe$_2$ (c,d) materials for RhB and Cr(VI) simultaneous removal.
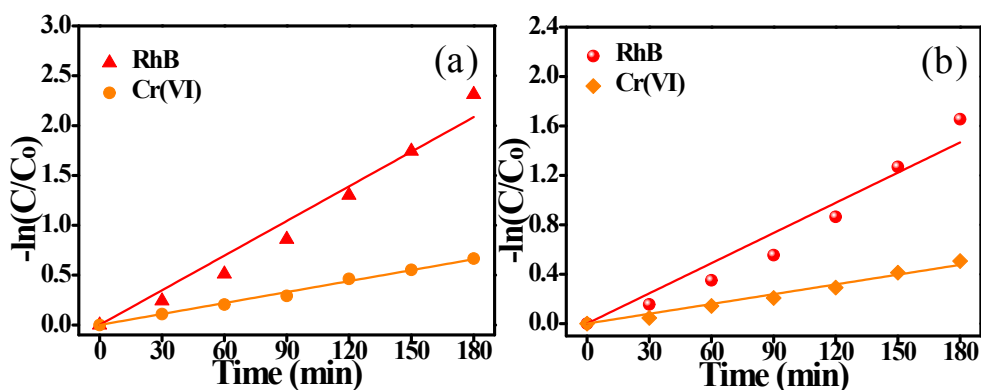

Fig. S16 The RhB and Cr(VI) removal rate constant for the (a) FeS-FeSe$_2$ and (b) FeSe$_2$.

The carrier density N$_D$ of the as-prepared photoanodes can be calculated from M-S curves according to the following Equation S1:[1,2]

$$N_D = \frac{2}{e\varepsilon_0\varepsilon}\left(\frac{dE}{d(\frac{1}{C^2})}\right) \tag{S1}$$

Where, C is the capacitance obtained from different potential with a fixed frequency (1000Hz), e is the electron charge (e=1.6×10^{-19} C), ε_0 is the vacuum permittivity (ε_0=8.86×10^{-19} F m^{-1}), and ε is the dielectric constant of FeSe$_2$ ($\varepsilon \approx 5.78$).
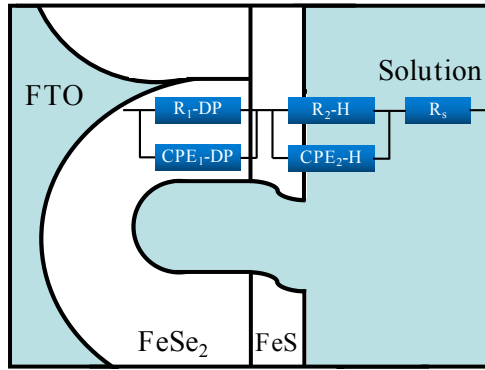
Fig. S17 The corresponding equivalent circuit models used for EIS data fitting.

The electron lifetime (τ_n) of as-prepared $FeSe_2$ and $FeS-FeSe_2$ photoanodes can be calculated by using the Bode phase plots, according to the following equation S2:[3]

$$\tau_n = \frac{1}{2\pi f_n} \tag{S2}$$

Where, τ_1 and f_1 are the electron lifetime and corresponding frequency at space charge layer, respectively; τ_2 and f_2 are the electron lifetime and corresponding frequency at double charge layer, respectively.

Table S3. The equivalent circuit parameters for pure $FeSe_2$ and $FeS-FeSe_2$ photoanode.

Sample	Solution	Space charge layer			Double charge layer		
	R_s (Ω)	R_1-DP (Ω)	CPE_1-DP (μF)	Electron lifetime (ms)	R_2-DP (Ω)	CPE_2-DP (μF)	Electron lifetime (ms)
$FeSe_2$	37.9	595.3	10.8	1.62	1281.0	14.4	7.41
$FeS-FeSe_2$	37.0	227.0	119	1.93	1027.0	44.8	9.71

According to the fitted results of time-resolved transient PL decay curves, the average decay lifetime (τ) of the as-obtained samples is calculated by the following Equation S3:[4]

$$\tau = \tau_1 A_1 + \tau_2 A_2 \tag{S3}$$

Where, τ is the average decay lifetime, τ_1 and A_1 are the fast decay component, τ_2 and A_2 are the minority-slow component, respectively.
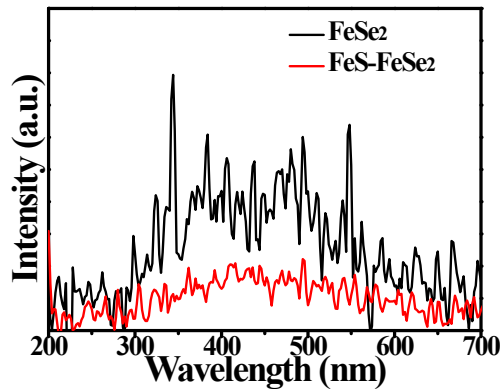
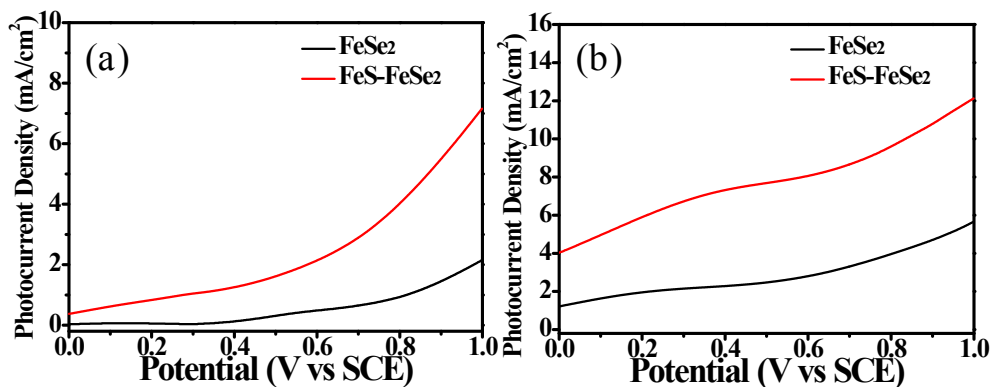

Fig. S18 The PL spectra of $FeSe_2$ and $FeS-FeSe_2$ samples.

Fig. S19 Linear sweep voltammetry for $FeSe_2$ and $FeS-FeSe_2$ measured in 0.5 M Na_2SO_4 (a) as well as in 0.35 M Na_2S and 0.25 M Na_2SO_3 solution (b) under solar light irradiation.

Table S4. Photocurrent density-applied potential for $FeSe_2$ and $FeS-FeSe_2$ photoanode in the present and absence of the hole scavengers.

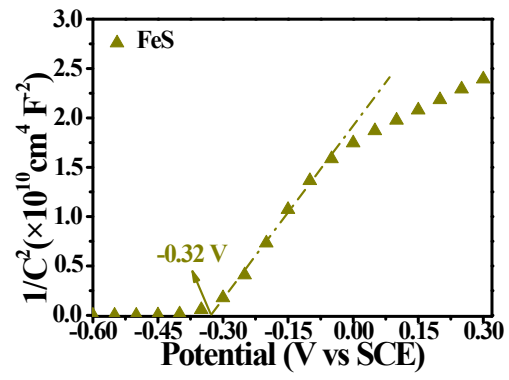| Potential	J (mA/cm^2, Na$_2$SO$_4$)		J (mA/cm^2, Na$_2$S/Na$_2$SO$_3$)	
(V vs SCE)	FeSe$_2$	FeS-FeSe$_2$	FeSe$_2$	FeS-FeSe$_2$
0.3	0.0359	1.05	2.15	6.72
0.35	0.0659	1.13	2.22	7.05
0.4	0.1259	1.26	2.28	7.31
0.45	0.206	1.42	2.36	7.52
0.5	0.306	1.62	2.47	7.68
0.55	0.406	1.86	2.62	7.85
0.6	0.486	2.14	2.80	8.06
0.65	0.556	2.48	3.03	8.31
0.7	0.646	2.89	3.31	8.66
0.75	0.766	3.41	3.62	9.08
0.8	0.936	4.02	3.96	9.60
0.85	1.17	4.72	4.32	10.18
0.9	1.45	5.49	4.70	10.78
0.95	1.79	6.32	5.14	11.46
1.0	2.15	7.16	5.66	12.12

Fig. S20 Mott-Schottky plots for pure FeS material.

References

1   M. Ye, J. Gong, Y. Lai, C. Lin and Z. Lin, *J. Am. Chem. Soc.*, 2012, **134**, 15720-15723.

2   Y. H. Chiu, K. D. Chang and Y. J. Hsu, *J. Mater. Chem. A*, 2018, **6**, 4286-4296.

3   H. Wang, Y. H. Liang, L. Liu, J. S. Hu, P. Wu and W. Q. Cui, *Appl. Catal. B-Environ.,* 2017, **208**, 22-34.

4   W. T. Bi, L. Zhang, Z. T. Sun, X. G. Li, T. Jin, X. J. Wu, Q. Zhang, Y. Luo, C. Z. Wu and Y. Xie, *ACS Catal.*, 2016, **6**, 4253-4257.